Acta Oceanol. Sin., 2019, Vol. 38, No. 1, P. 71–77
https://doi.org/10.1007/s13131-019-1371-0
http://www.hyxb.org.cn
E-mail: hyxbe@263.net

Geochemistry and age of seamounts in the West Pacific: mantle processes and petrogenetic implications

Limei Tang[1, 2], Yanhui Dong[1, 2*], Fengyou Chu[1, 2], Ling Chen[1, 2], Weilin Ma[1, 2], Yonggang Liu[3]

[1] Key Laboratory of Submarine Geosciences, Ministry of Natural Resources, Hangzhou 310012, China

[2] Second Institute of Oceanography, Ministry of Natural Resources, Hangzhou 310012, China

[3] Guangzhou Marine Geological Survey, Ministry of Natural Resources, Guangzhou 510760, China

Received 3 May 2017; accepted 20 October 2017

Abstract

Research on seamounts provides some of the best constraints for understanding intraplate volcanism, and samples from seamounts reveal crucial evidence about the geochemical makeup of the oceanic mantle. There are still many seamounts in the West Pacific Seamount Province (WPSP) that have not been studied, meaning their ages and geochemistry remain unknown. A better understanding of these seamount trails and their evolutionary history, investigated with age and geochemistry data, will enable better understanding of the geological processes operating underneath the Pacific Ocean Plate. Here, new $^{40}Ar/^{39}Ar$ ages and trace element and Sr-Nd-Pb isotopic data for seven basalt rocks from four seamounts in the WPSP are provided. Chemically, these rocks are all Oceanic Island Alkali basalt (OIA type); analysis of olivine phenocrysts shows that the magmas experienced strong olivine fractionation and changed from olivine + plagioclase to olivine + plagioclase + clinopyroxene cotectic during their evolution. Rare earth element (REE) patterns and a spider diagram of the samples in this study show OIB (Ocean Island Basalt) like behavior. The range of $^{87}Sr/^{86}Sr$ values is from 0.704 60 to 0.706 24, the range of $^{206}Pb/^{204}Pb$ values is from 18.241 to 18.599, and the range of $^{143}Nd/^{144}Nd$ values is from 0.512 646 to 0.512 826; together, these values indicate magma sources ranging from EMI to EMII. Finally, new $^{40}Ar/^{39}Ar$ age data show that these seamounts formed at ~97 and ~106 Ma, indicating that some may have undergone the same formation processes as seamounts in the eastern part of the Magellan Seamount Trail, but other seamounts likely have different origins.

Key words: $^{40}Ar/^{39}Ar$ ages, geochemistry, magmatic evolution, basalts, West Pacific

Citation: Tang Limei, Dong Yanhui, Chu Fengyou, Chen Ling, Ma Weilin, Liu Yonggang. 2019. Geochemistry and age of seamounts in the West Pacific: mantle processes and petrogenetic implications. Acta Oceanologica Sinica, 38(1): 71–77, doi: 10.1007/s13131-019-1371-0

1 Introduction

Since the publication of the deep-rooted mantle plume hypothesis (Morgan, 1971, 1972) and the elegant explanation of volcanic age progression of the Hawaii–Emperor seamount chain in the Pacific (Clague and Dalrymple, 1989), mantle plumes and hotspots have been widely used to explain mantle anomalies within the interior of a plate. However, over the past two decades, the hotspot hypothesis has been subjected to several critical re-evaluations (Anderson, 2002, 2005, 2007; Hamilton, 2003; Foulger, 2002, 2010; Foulger and Natland, 2003; Koppers et al., 2003; Koppers and Staudigel, 2005; Natland and Winterer, 2005; Tarduno et al., 2009). Understanding the nature of hotspot volcanism is important because hotspot trails are used to determine the absolute motion of lithospheric plates through geological time, and also because the hotspots are an important means of heat transport between the deep mantle and the earth's lithosphere (Koppers et al., 1998, 2000, 2003, 2004; Koppers and Staudigel, 2005; White, 2005; Chu et al., 2005). Seamounts offer the best direct evidence of intraplate volcanism originating from the mantle beneath; when seamounts erupt, they are the best indicators of how the lithosphere in their local tectonic setting interacts with magma originating from the deep mantle (Hillier, 2007). Rocks and minerals from seamounts can therefore provide insights into geological processes in the deep mantle.

There are many seamounts distributed in the West Pacific Seamount Province (WPSP) (Chu et al., 2006; He et al., 2011; Zhao et al., 2014; Huo et al., 2015), a region that is characterized by an unusually shallow seafloor (Menard, 1964) and an unusually large number of intraplate volcanic edifices formed between 138 and 60 Ma (Lincoln et al., 1993). Some of these seamounts follow a trail pattern while others do not; for example, three seamounts (Vlinder, Pako, Loah) in the Magellan Seamount Trail (MST) show regular age decline, but others show no such pattern (e.g., Ita Mai Tai). The MST is therefore defined as a complex, short and discontinuous chain of guyots. Plate tectonic reconstructions of the Pacific region indicate that the lithosphere in the WPSP originated above the South Pacific Thermal and Isotopic Anomaly (SOPITA) region of the deeper mantle (Koppers et al., 1995), and the mantle source of the WPSP is also identified as a Cretaceous isotopic equivalent of the SOPITA (Smith et al.,

Foundation item: The National Basic Research Program (973 Program) of China under contract No. 2015CB755905; the National Natural Science Foundation of China under contract No. 41506070; the Scientific Research Fund of the Second Institute of Oceanography, SOA under contract Nos JG1803, JG1603 and JG1403; the Natural Science Foundation of Zhejiang Province of China under contract No. LQY18D060002.

*Corresponding author, E-mail: luster15991@163.com

1989; Staudigel et al., 1991). However, many seamounts remain unstudied, particularly those in the Northwest Pacific near the Mariana Trench; it is thus unclear whether these seamounts are the same as other WPSP seamounts in having origins above the SOPITA. It is also unclear whether these seamounts were formed by hotspots or by lithospheric extension driven by subduction. In this study, we present new age, geochemical, mineralogical and isotopic composition data from four seamounts in the WPSP that are located near the Mariana Trench. We compare these data with data from the MST to determine whether these seamounts show any relationships with the MST. We also discuss the mantle processes associated with these seamounts.

2 Samples and analytical methods

2.1 *Geochemistry*

The rock samples for this study were obtained by deep dredging of the northwestern part of the MST area during the DY115–19 and DY125–31 cruises. As shown in Fig. 1, a total of seven basaltic lava samples were selected: MID20, MID23, MID24, MJD03, MKD03, MDD47 and MDD53. Back-scatter electron (BSE) images and mineralogical analyses of theses samples were obtained with a JOELJXA-8100 microprobe, located at the Key Laboratory of Submarine Geosciences, Ministry of Natural Resources, Hangzhou. Major and trace elements were analyzed at the Guangzhou Institute of Geochemistry, Chinese Academy of Sciences, with an Axios sequential X-ray fluorescence spectrometer and ICP-MS (Agilent 7500). Sr-Nd-Pb isotope analysis was performed with a multi-collector ICP-MS (Neptune MC-ICP-MS, Thermo Scientific), using internal standardization and external calibration with bracketing isotope standard reference materials (ALS Scandinavia, Luleå, Sweden). Sr and Nd isotope ratios were normalized to $^{86}Sr/^{88}Sr$=0.119 4 and $^{146}Nd/^{144}Nd$=0.721 9, respectively. During the analyses, the Nd isotope standard *Thermo Nd* yielded an $^{143}Nd/^{144}Nd$ ratio of 0.512 420±0.000 009 (2σ, n=2), and the Sr isotope standard *NBS987* yielded an $^{87}Sr/^{88}Sr$ value of 0.710 266±0.000 006 (2σ, n=2). The measured $^{206}Pb/^{204}Pb$, $^{207}Pb/^{204}Pb$ and $^{208}Pb/^{204}Pb$ ratios of the standard *NBS981* were 16.937 4±0.008 5, 15.491 6±0.007 6 and 36.721 9±0.018 2 (2σ, n=2), respectively. Standard deviations are reported from repeated analyses of each sample.

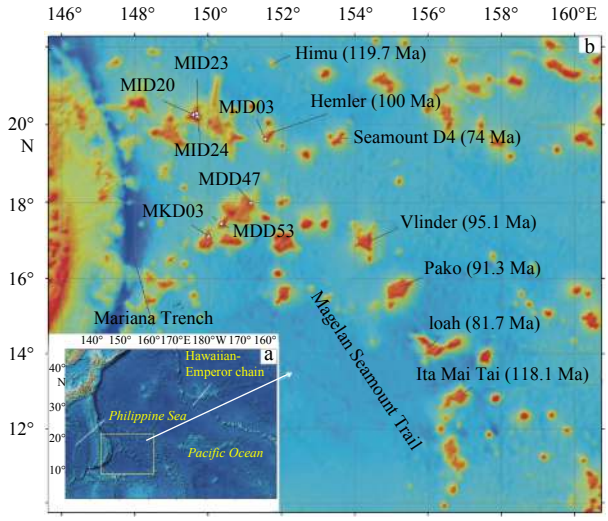

Fig. 1. Regional geological map (a) and Location of the samples of this study from seamounts in West Pacific Seamount Province (WPSP) (b).

2.2 *$^{40}Ar/^{39}Ar$ geochronology*

Samples were crushed and sieved into 250 to 125 mm and 150 to 74 mm size fractions. Plagioclase was separated from the 250 to 125 mm fraction using a paramagnetic separator, and from the 150 to 74 mm fraction using a combination of heavy liquid and paramagnetic methods. Samples were cleaned with mixtures of HF, HCl and HNO_3 before final washing in distilled H_2O in an ultrasonic bath.

Samples were irradiated in the cadmium-shielded CLICIT facility at the TRIGA reactor at Oregon State University and incrementally heated at the laser probe dating facility at VU University, Amsterdam. Methods used for data acquisition and reduction, mass discrimination correction, and age calculation followed those previously described in detail by Koppers et al. (2000) and Koppers (2002). Ages were calculated using the freeware program ArArCALC (Koppers, 2002); a detailed description of this method is found in the supporting information of Koppers et al. (2012).

3 Results

3.1 *Geochemistry*

The results of major and trace element analyses are presented in Table 1, and isotopic data is provided in Table 2. Representative electron probe micro-analyzer (EPMA) results from olivine phenocrysts in seamount basalts are presented in Table 3; Figure 2 shows micrographs of olivine phenocrysts. The MgO content shows a large range from 2.20% to 9.06%, and Mg# [$Mg^{2+}/(Mg^{2+}+Fe^{2+})$] is from 0.13 to 0.39, indicative of strong magma fractionation. The TiO_2 content is high (generally greater than 2%), as is the Fe_2O_3 content (average value 13.27%). The basaltic samples of the Magellan seamount are all classified as alkaline and fall in the Oceanic Island Alkali (OIA) basalt range (Fig. 3). The REE pattern and spider diagram of the samples in this study show OIB-like patterns (Fig. 4). The range of $^{87}Sr/^{86}Sr$ is 0.704 60 to 0.706 24, for $^{206}Pb/^{204}Pb$, it is 18.241 to 18.599, and for $^{143}Nd/^{144}Nd$, it is 0.512 646 to 0.512 826.

3.2 *$^{40}Ar/^{39}Ar$ ages*

The ages of two fresh samples, MID20 and MKD03, were determined. The incremental heating technique was used to slowly degas grains to remove alterations typically present in the lower temperature steps (e.g., Koppers et al., 2000, 2004). These results (Table 4) confidently indicate eruption ages of (106.32±0.4) Ma for the seamount that MID20 erupted from and (97.93±0.31) Ma for the seamount from which MK03 erupted (Fig. 5).

4 Discussion

4.1 *Magma evolution*

Olivine crystals can precipitate directly from magma (Echeverría and Aitken, 1986), as well as in the form of exotic xenocrysts (Révillon et al., 1999) derived from mantle peridotites (Zhang, 2005) or from previously unerupted magma (Thompson and Gibson, 2000). Magmatic olivine is associated with mantle-melting events (Nisbet et al., 1993), whereas olivine xenocrysts from mantle peridotite may reflect the compositional characteristics of the lithospheric mantle because they are captured from the lithospheric mantle during magma ascent (Zhang, 2005). Research on olivine phenocrysts thus provides useful information about both the magma's source and its evolution.

Table 1. The major (%), trace element and REE ($\times 10^{-6}$) data of the samples from WPSP of this study

Sample	MDD47	MDD53	MID20	MID23	MID24	MJD03	MKD03
Al_2O_3	19.49	16.30	15.13	14.41	12.61	13.74	15.31
CaO	8.00	6.11	10.97	12.10	12.60	10.43	9.81
Fe_2O_3	8.79	11.63	16.11	14.60	13.52	14.62	13.62
K_2O	2.09	2.11	1.17	1.33	0.60	2.06	1.25
MgO	4.14	3.38	4.42	6.39	9.06	2.20	5.72
MnO	0.22	0.12	0.12	0.20	0.18	0.27	0.14
Na_2O	2.31	3.07	2.14	1.46	2.86	2.53	2.67
P_2O_5	1.55	1.03	1.08	0.81	0.69	1.10	0.92
SiO_2	44.05	48.48	41.44	41.45	40.97	43.58	44.03
TiO_2	1.74	2.52	2.11	2.14	2.45	2.75	2.61
LOI	7.03	4.63	4.69	4.47	3.82	6.13	3.28
Total	99.41	99.38	99.38	99.38	99.37	99.40	99.37
$Mg^{\#}$	0.31	0.22	0.21	0.29	0.39	0.13	0.29
Sc	16.98	25.64	29.19	41.25	28.61	32.26	23.34
Ti	10 892.4	14 490.0	12 663.6	14 085.2	14 320.2	18 961.7	15 741.9
V	141.0	85.8	311.3	281.9	231.6	263.3	212.4
Cr	143.0	306.2	669.6	532.1	640.5	692.0	243.7
Mn	1 853.6	1 015.8	957.0	1 661.0	1 262.0	5 005.2	1 174.3
Co	33.88	58.11	34.67	58.97	51.56	166.20	50.53
Ni	107.6	227.5	195.6	151.7	287.0	383.5	186.2
Cu	213.6	443.6	220.1	137.6	104.5	546.4	287.9
Zn	186.9	485.2	351.8	184.6	139.6	464.0	396.8
Ga	29.11	22.15	20.86	16.53	17.15	18.28	22.43
Ge	2.477	1.052	1.468	3.815	1.693	2.320	1.621
Rb	59.09	46.21	23.22	30.24	15.67	36.39	22.32
Sr	726.8	494.2	469.9	576.8	626.0	282.9	827.1
Y	63.20	41.36	57.36	47.02	30.16	33.76	26.89
Zr	584.7	205.6	164.7	181.8	201.7	263.0	170.9
Nb	131.80	28.87	45.67	74.59	101.70	68.59	45.07
Cs	0.798	2.106	1.203	1.022	5.383	1.133	0.967
Ba	788.4	248.0	319.4	279.6	689.7	234.2	674.5
La	140.3	34.13	53.11	72.25	86.43	44.30	40.80
Ce	219.3	67.99	87.81	130.10	156.50	94.51	79.61
Pr	21.77	8.064	9.032	13.640	16.720	11.770	9.389
Nd	70.37	34.74	36.46	49.86	59.39	47.58	37.75
Sm	10.36	7.673	6.989	9.205	9.643	9.842	7.470
Eu	2.638	2.491	2.200	2.912	2.771	2.896	2.464
Gd	8.676	7.228	7.509	8.638	7.738	9.225	6.726
Tb	1.324	1.113	1.111	1.288	1.106	1.272	0.952
Dy	7.885	6.327	6.708	7.630	6.157	6.920	5.002
Ho	1.701	1.311	1.411	1.543	1.165	1.308	0.984
Er	4.705	3.443	3.803	4.110	2.997	3.176	2.358
Tm	0.694	0.482	0.530	0.581	0.396	0.426	0.308
Yb	4.456	3.097	3.241	3.657	2.487	2.616	1.890
Lu	0.697	0.460	0.478	0.546	0.353	0.367	0.281
Hf	12.000	4.536	3.671	3.992	4.458	5.727	3.871
Ta	9.638	1.923	2.658	4.604	5.822	3.936	2.785
Pb	25.460	22.210	15.630	12.850	6.825	51.190	15.720
Th	42.31	3.475	4.404	10.210	12.430	7.954	5.001
U	2.816	1.184	1.324	1.212	2.449	0.895	1.192

Note: LOI is abbreviated from loss on ignition.

Magmatic olivine phenocrysts and mantle peridotite-derived olivine xenocrysts have distinct differences in a chemical composition (Wang et al., 2013). The CaO content of the former is significantly higher than that of the latter (Francis, 1985; Gurenko et al., 1996; Thompson and Gibson, 2000). The low CaO content of olivine xenocrysts derived from a mantle peridotite source, typically substantially less than 0.1% (Gurenko et al., 1996; Thompson and Gibson, 2000; Hirano et al., 2004), results from the control of the CaO content, crystallization pressure, temperature, and oxygen fugacity of the olivine crystals by the CaO and FeO contents of magmatic melts (Jurewicz and Watson, 1998; Libourel, 1999; Liu et al., 2013). The low CaO content and high Mg# of mantle

Table 2. The isotopic data of the samples from seamounts of this study

Sample	$^{206}Pb/^{204}Pb$	$^{208}Pb/^{204}Pb$	$^{207}Pb/^{204}Pb$	$^{87}Sr/^{86}Sr$	$^{143}Nd/^{144}Nd$
MJD03	18.432±21	38.468	15.617	0.706 24±15	0.512 701±9
MKD03	18.241±16	38.257	15.614	0.704 60±23	0.512 646±8
MID23	18.599±15	38.666	15.624	0.704 61±25	0.512 826±7

Table 3. Representative EPMA results (%) of olivine phenocrysts in basalts from the Seamounts of this study

Element	MID23–6	MID23–7	MID23–10	MID23–12	MJD03–1	MJD03–2	MJD03–11	MJD03–12	MJD03–14	MJD03–16	MJD03–18
SiO_2	40.24	40.14	40.16	39.98	40.24	40.19	39.47	39.71	38.51	0.01	38.80
TiO_2	0	0	0.01	0.06	0.02	0.03	0.01	0.03	0.04	0.007	0.03
Al_2O_3	0.05	0.07	0.04	0.07	0.06	0.04	0.06	0.07	0.31	0.087	0.09
Cr_2O_3	0.06	0	0.26	0.09	0.14	0.03	0.15	0.29	0.12	45.23	0.49
FeO	12.25	14.51	13.11	14.71	13.77	13.36	13.84	12.28	15.45	0.54	12.27
MnO	0.24	0.24	0.25	0.28	0.13	0.12	0.23	0.15	0.18	0.17	0.19
MgO	47.19	44.91	46.26	45.05	46.03	46.31	44.68	46.37	43.35	0.06	45.59
CaO	0.33	0.39	0.33	0.38	0.25	0.22	0.61	0.20	0.59	0	0.20
Na_2O	0.02	0.01	0	0.02	0.01	0.04	0	0.01	0.04	14.42	0.01
K_2O	0	0	0	0.01	0.01	0.01	0.01	0	0.03	39.06	0
NiO	0.27	0.21	0.20	0.15	0.17	0.23	0.10	0.26	0.09	0.116	0.25
Total	100.66	100.49	100.61	100.80	100.83	100.56	99.18	99.37	98.71	99.70	97.92
Fo	87	85	86	85	86	86	85	87	83	85	87

Note: Fo=100 Mg/(Mg+Fe)

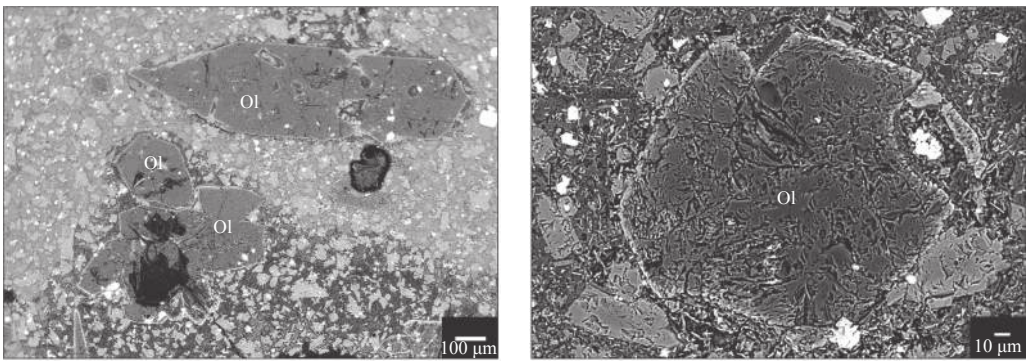

Fig. 2. Photomicrographs of olivine phenocrysts.

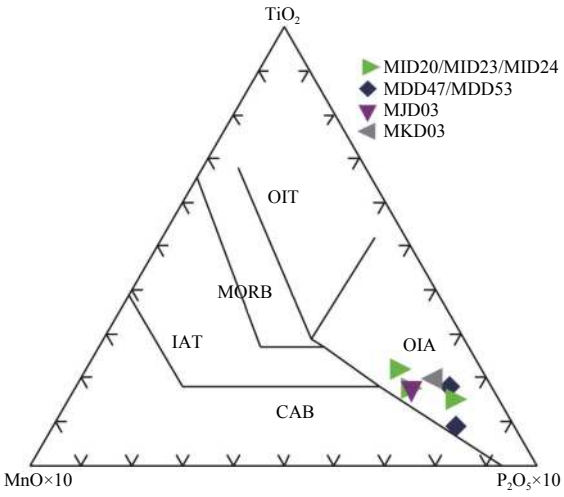

Fig. 3. Na_2O+K_2O-Si_2O and TiO_2-MnO×10-P_2O_5×10 diagram of basalts from the seamounts of this study.

peridotites results in very low CaO contents in olivine xenocrysts. Because the CaO content of olivine phenocrysts in the basalt samples from the Magellan Seamounts is typically higher than 0.1% (Fig. 6a), a mantle peridotite source can be ruled out. The relationship between the CaO and NiO contents and the forsterite (Fo) content also suggests a magmatic origin for the olivine. The NiO content of the olivine is consistent with a decrease in the Fo content that deviates significantly from typical trends of mantle peridotites, but instead follows a trend typically indicative of magmatic fractionation (Fig. 6b) (Sato, 1977).

Fe-Mg partition coefficients between olivine and magmatic melt are commonly used to investigate whether the olivine phenocrysts are equilibrated to the whole rock Mg# values (Nisbet et al., 1993; Thompson and Gibson, 2000). If magmas do not undergo fractional crystallization or crystal accumulation, the olivine composition and the whole-rock Mg# would constitute an equilibrium curve. The olivine richest in Mg that crystallized in equilibrium with the initial magma should fall within the range of the equilibrium curve; olivine that crystallized from evolved magma would fall below the equilibrium curve. Meanwhile, olivine xenocrysts may fall above or below the equilibrium curve depending on their source characteristics (Révillon et al., 1999). The olivine phenocrysts in the Magellan Seamount basalts studied here consistently fall below the equilibrium curve (Fig. 7a), suggesting that they are the result of crystallization from the same (subsequently fractionated) magma as the whole rock.

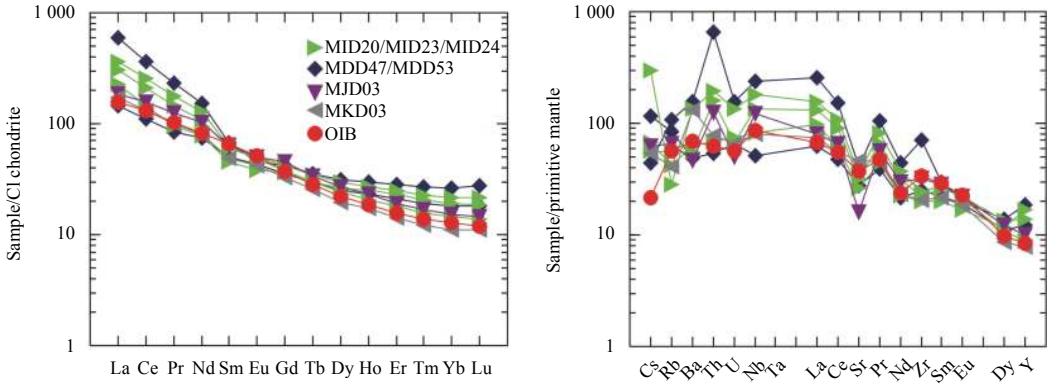

Fig. 4. The REE pattern and spider diagram of basalts of this study.

Table 4. $^{40}Ar/^{39}Ar$ age results of basalt in this study

Sample	Material	Age type	Age/Ma±2σ	K/Ca±2σ
MID20	groundmass	eprution age	106.32±0.36	0.035 4±0.000 1
MK03	groundmass	eprution age	97.93±0.31	0.103±0.013

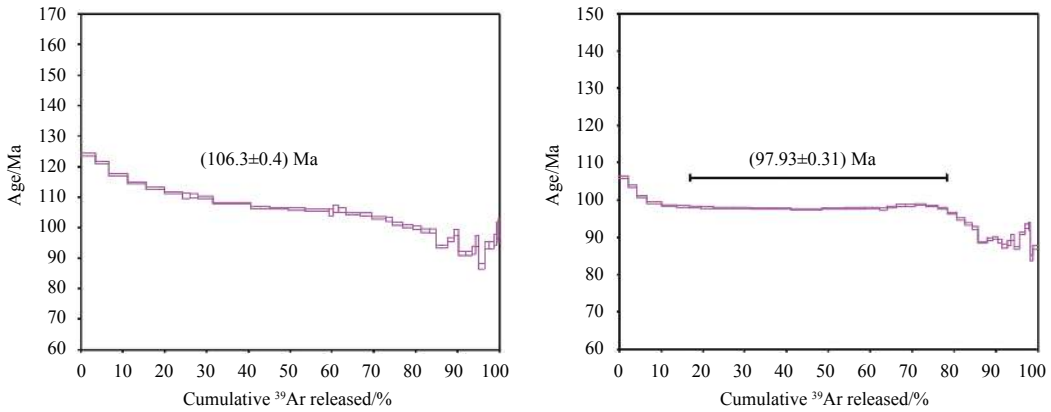

Fig. 5. High-resolution incremental heating $^{40}Ar/^{39}Ar$ age analyses for the basalts.

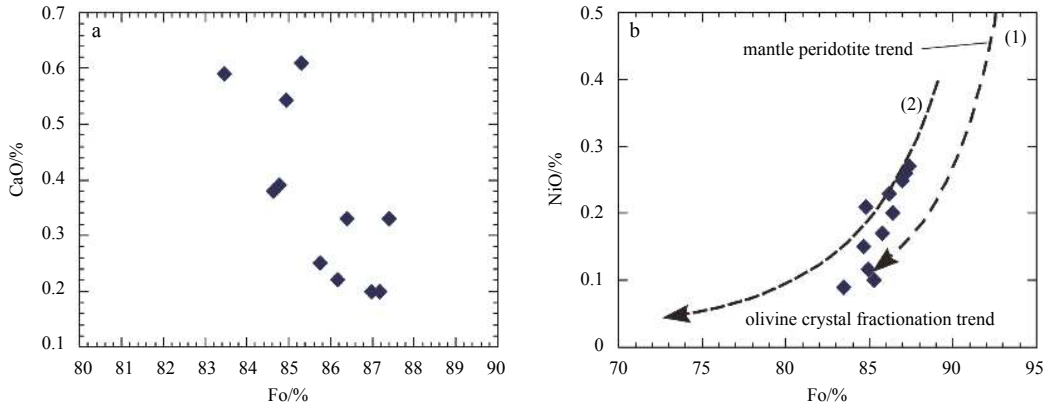

Fig. 6. Correlation diagram of Fo-CaO (a) and Fo-NiO (b).

The basalts from the western part of the MST show a positive correlation of CaO with MgO at MgO<8.0% (Fig. 7b), suggesting that the magma forming the Magellan Seamounts changed from the olivine+plagioclase to the olivine+plagioclase+clinopyroxene cotectic, because the much higher CaO content of clinopyroxene than that of olivine and plagioclase means that clinopyroxene fractionation would be associated with a decrease in magma CaO concentration.

4.2 *Magma source*

Most basalts from seamounts in the Pacific Ocean are OIBs, but their magma source differs between EMI, EMII and HIMU. As illustrated in Fig. 8, $^{87}Sr/^{86}Sr$-$^{206}Pb/^{204}Pb$ and $^{143}Nd/144Nd$-$^{87}Sr/^{86}Sr$ values indicate that different seamount trails in the Pacific Ocean have different magma sources (Koppers et al., 2003). Considering samples in this study from the western part of the MST, the seamounts from which samples MKD03 and MID20

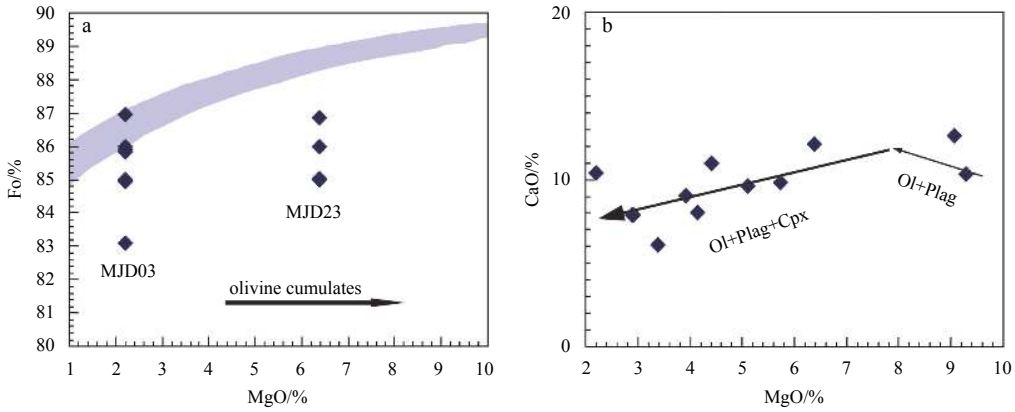

Fig. 7. Correlation diagram of Fo-MgO (a) and CaO-MgO (b). The shaded area is olivine composition range of balanced with whole-rock MgO content (Sato, 1977). Ol represents olivine, Plag plagioclase and Cpx Clinopyroxene.

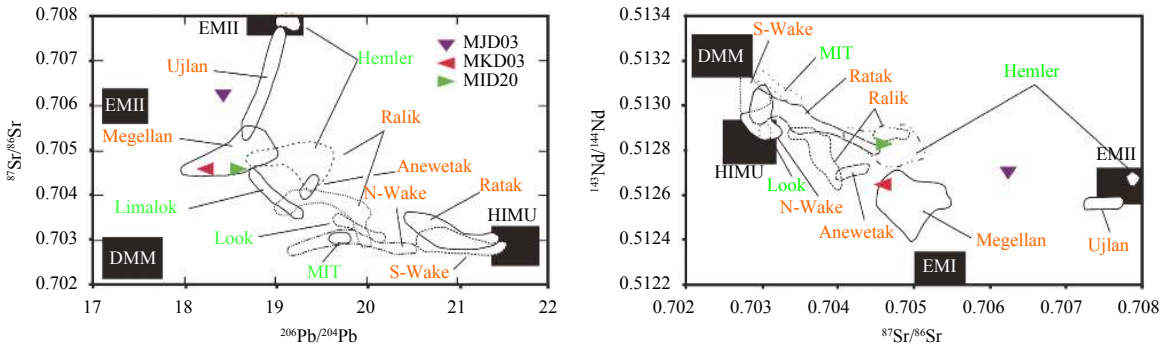

Fig. 8. The $^{87}Sr/^{86}Sr$-$^{206}Pb/^{204}Pb$ diagram and $^{143}Nd/^{144}Nd$-$^{87}Sr/^{86}Sr$ diagram and of samples from the west part of MST (after Koppers et al., 2003).

were obtained may have a similar magma source to MST and Hemler (EMI), but the seamount from which sample MJD03 was obtained has a different magma source to MST that is an intermediate between EMI and EMII. This may suggest that the two seamounts from which MJD03 and MID20 were obtained belong to the MST trail, but that the seamounts from which MJD03 was obtained does not.

4.3 *Formation implications*

The seamounts that from which MKD03 and MID20 were obtained have ages of 97 and 106 Ma, respectively. Therefore, these follow the same linear age trend as seamounts in the eastern part of the MST such as Vlinder, Pako, and Loah, and have a similar magma source; this suggests that they belong to the MST and underwent the same petrogenetic processes in the Cretaceous South Pacific SOPITA, before moving to their present location (Koppers et al., 1998). Meanwhile seamount Hemler, of age 100 Ma, has a different mantle source from the MST, with a reduced bulk earth component compared with the MST, and was likely formed by different processes, e.g., lithospheric extension; alternatively, it may instead belong to another seamount trail containing other low-volume seamounts nearby.

5 Conclusions

OIA-type magmas that formed basalts in the western part of the MST, in the West Pacific Seamount Province, experienced strong olivine fractionation, and moved from the olivine+plagioclase to the olivine+plagioclase+clinopyroxene cotectic during their evolution. Some of the seamounts have an EMI type magma source like the MST, but others have a magma source intermediate between EMI and EMII. New $^{40}Ar/^{39}Ar$ ages show that these seamounts formed at ~97 Ma and ~106 Ma. Our results indicate that while some seamounts may have been formed through the same petrogenetic processes as the eastern part of the MST, others may have different origins.

Acknowledgements

We are thankful to the crew and scientists involved with the DY115–19 cruise and the first cruise of the *Jiaolong* submersible with experimental applications. We appreciate the help of Ying Liu of Guangzhou Institute of Geochemistry, the Chinese Academy of Sciences, for the major elements analysis.

References

Anderson D L. 2002. Plate tectonics as a far-from-equilibrium self-organized system. In: Stein S, Freymueller J T, eds. Plate Boundary Zones. Washington: AGU, 411–425

Anderson D L. 2005. The plume assumption: frequently used arguments. http://www.mantleplumes.org/FUA.html, [2016–08–10]

Anderson D L. 2007. New Theory of the Earth. 2nd ed. Cambridge: Cambridge University Press, 384

Chu Fengyou, Chen Jianlin, Ma Weilin, et al. 2005. Petrologic characteristics and ages of basalt in middle Pacific mountains. Marine Geology & Quaternary Geology (in Chinese), 25(4): 55–59

Chu Fengyou, Sun Guosheng, Ma Weilin, et al. 2006. Classification of seamount morphology and its evaluating significance of ferromanganese crust in the central Pacific Ocean. Acta Oceanologica Sinica, 25(2): 63–70

Clague D A, Dalrymple G B. 1989. Tectonics, geochronology, and ori-

gin of the Hawaiian-Emperor volcanic chain. In: Winterer E L, Hussong D M, Decker R W, eds. The Eastern Pacific and Hawaii. The Geological Society of America, Boulder, Colorado, USA. 188–217

Echeverría L M, Aitken B G. 1986. Pyroclastic rocks: another manifestation of ultramafic volcanism on Gorgona Island, Colombia. Contributions to Mineralogy and Petrology, 92(4): 428–436, doi: 10.1007/BF00374425

Foulger G R. 2002. Plumes, or plate tectonic processes?. Astronomy & Geophysics, 43(6): 19–23

Foulger G R. 2010. From plate tectonics to plumes, and back again. In: Foulger G R, ed. Plates VS. Plumes: A Geological Controversy. Chichester, UK: John, Wiley & Sons, Inc., doi: 10.1002/9781444324860.ch1

Foulger G R, Natland J H. 2003. Is "hotspot" volcanism a consequence of plate tectonics?. Science, 300(5621): 921–922, doi: 10.1126/science.1083376

Francis D. 1985. The Baffin Bay lavas and the value of picrites as analogues of primary magmas. Contributions to Mineralogy and Petrology, 89(2–3): 144–154, doi: 10.1007/BF00379449

Gurenko A A, Hansteen T H, Schmincke H U. 1996. Evolution of parental magmas of Miocene shield basalts of Gran Canaria (Canary Islands): constraints from crystal, melt and fluid inclusions in minerals. Contributions to Mineralogy and Petrology, 124(3–4): 422–435, doi: 10.1007/s004100050201

Hamilton W B. 2003. An alternative earth. GSA Today, 13(11): 4–12, doi: 10.1130/1052-5173(2003)013<0004:AAE>2.0.CO;2

He Gaowen, Ma Weilin, Song Chengbing, et al. 2011. Distribution characteristics of seamount cobalt-rich ferromanganese crusts and the determination of the size of areas for exploration and exploitation. Acta Oceanologica Sinica, 30(3): 63–75, doi: 10.1007/s13131-011-0120-9

Hillier J K. 2007. Pacific seamount volcanism in space and time. Geophysical Journal International, 168(2): 877–889, doi: 10.1111/gji.2007.168.issue-2

Hirano N, Yamamoto J, Kagi H, et al. 2004. Young, olivine xenocryst-bearing alkali-basalt from the oceanward slope of the Japan Trench. Contributions to Mineralogy and Petrology, 148(1): 47–54, doi: 10.1007/s00410-004-0593-z

Huo Yingyi, Cheng Hong, Post A F, et al. 2015. Ecological functions of uncultured microorganisms in the cobalt-rich ferromanganese crust of a seamount in the central Pacific are elucidated by fosmid sequencing. Acta Oceanologica Sinica, 34(4): 92–113, doi: 10.1007/s13131-015-0650-7

Jurewicz A J G, Watson E B. 1988. Cations in olivine, Part 1: Calcium partitioning and calcium-magnesium distribution between olivines and coexisting melts, with petrologic applications. Contributions to Mineralogy and Petrology, 99(2): 176–185, doi: 10.1007/BF00371459

Koppers A A P. 2002. ArArCALC-Software for $^{40}Ar/^{39}Ar$ age calculations. Computers & Geosciences, 28(5): 605–619

Koppers A A P, Duncan R A, Steinberger B. 2004. Implications of a nonlinear $^{40}Ar/^{39}Ar$ age progression along the Louisville seamount trail for models of fixed and moving hot spots. Geochemistry, Geophysics, Geosystems, 5(6): Q06L02, doi: 10.1029/2003GC000671

Koppers A A P, Staudigel H. 2005. Asynchronous bends in Pacific seamount trails: a case for extensional volcanism?. Science, 307(5711): 904–907, doi: 10.1126/science.1107260

Koppers A A P, Staudigel H, Christie D M, et al. 1995. Sr-Nd-Pb isotope geochemistry of leg 144 West Pacific Guyots: implications for the geochemical evolution of the "SOPITA" mantle anomaly. In: Haggerty J A, Premoli S I, Rack F, et al, eds. Proceedings of the Ocean Drilling Program, Scientific Results. College Station, Texas. 535–545

Koppers A A P, Staudigel H, Pringle M S, et al. 2003. Short-lived and discontinuous intraplate volcanism in the South Pacific: hot spots or extensional volcanism?. Geochemistry, Geophysics, Geosystems, 4(10): 1089

Koppers A A P, Staudigel H, Wijbrans J R, et al. 1998. The magellan seamount trail: implications for Cretaceous hotspot volcanism and absolute Pacific plate motion. Earth and Planetary Science Letters, 163(1-4): 53–68, doi: 10.1016/S0012-821X(98)00175-7

Koppers A A P, Staudigel H, Wijbrans J R. 2000. Dating crystalline groundmass separates of altered Cretaceous seamount basalts by the $^{40}Ar/^{39}Ar$ incremental heating technique. Chemical Geology, 166(1-2): 139–158, doi: 10.1016/S0009-2541(99)00188-6

Koppers A A P, Yamazaki T, Geldmacher J, et al. 2012. Limited latitudinal mantle plume motion for the Louisville hotspot. Nature Geoscience, 5(12): 911–917, doi: 10.1038/ngeo1638

Libourel G. 1999. Systematics of calcium partitioning between olivine and silicate melt: implications for melt structure and calcium content of magmatic olivines. Contributions to Mineralogy and Petrology, 136(1-2): 63–80, doi: 10.1007/s004100050524

Lincoln J M, Pringle M S, Silva I P. 1993. Early and late cretaceous volcanism and reef-building in the Marshall Islands. In: Pringle M S, Sager W W, Sliter W V, et al, eds. The Mesozoic Pacific: Geology, Tectonics, and Volcanism. The American Geophysical Union, Washington. 279–305

Liu Wenlong, Zhang Junfeng, Liu Chujian. 2013. CPO Induced seismic anisotropy in subduction zone: antigorite vs. olivine. Acta Geologica Sinica, 87(S1): 190

Menard H W. 1964. Marine Geology of the Pacific. New York: McGraw-Hill

Morgan W J. 1971. Convection plumes in the lower mantle. Nature, 230(5288): 42–43, doi: 10.1038/230042a0

Morgan W J. 1972. Deep mantle convection plumes and plate motions. AAPG Bulletin, 56(2): 203–213

Natland J H, Winterer E L. 2005. Fissure control on volcanic action in the Pacific. In: Foulger G R, Natland J H, Presnall D, et al, eds. Plates, Plumes, and Paradigms. Geological Society of America, Boulder. 687–710

Nisbet E G, Cheadle M J, Arndt N T, et al. 1993. Constraining the potential temperature of the Archaean mantle: a review of the evidence from komatiites. Lithos, 230(3-4): 291–307

Révillon S, Arndt N T, Hallot E, et al. 1999. Petrogenesis of picrites from the Caribbean Plateau and the North Atlantic magmatic province. Lithos, 49(1–4): 1–21, doi: 10.1016/S0024-4937(99)00038-9

Sato H. 1977. Nickel content of basaltic magmas: identification of primary magmas and a measure of the degree of olivine fractionation. Lithos, 10(2): 113–120, doi: 10.1016/0024-4937(77)90037-8

Smith W H F, Staudigel H, Watts A B, et al. 1989. The Magellan seamounts: early Cretaceous record of the south Pacific isotopic and thermal anomaly. Journal of Geophysical Research, 94(B8): 10501–10523, doi: 10.1029/JB094iB08p10501

Staudigel H, Park K H, Pringle M, et al. 1991. The longevity of the south Pacific isotopic and thermal anomaly. Earth and Planetary Science Letters, 102(1): 24–44, doi: 10.1016/0012-821X(91)90015-A

Tarduno J, Bunge H P, Sleep N, et al. 2009. The bent Hawaiian-Emperor hotspot track: inheriting the mantle wind. Science, 324(5923): 50–53, doi: 10.1126/science.1161256

Thompson R N, Gibson S A. 2000. Transient high temperatures in mantle plume heads inferred from magnesian olivines in Phanerozoic picrites. Nature, 407(6803): 502–506, doi: 10.1038/35035058

Wang Zhengrong, Qiu Lin, Zhang Shuang, et al. 2013. The reaction kinetics between CO_2-bearing fluid and olivines/Hawaiian picrites. Acta Geologica Sinica, 87(S1): 967–968

White S M. 2005. Seamounts. In: Selley R C, Cocks L R M, Plimer I R, eds. Encyclopedia of Geology. Amsterdam: Elsevier, 475–485

Zhang Hongfu. 2005. Transformation of lithospheric mantle through peridotite-melt reaction: a case of Sino-Korean craton. Earth and Planetary Science Letters, 237(3–4): 768–780, doi: 10.1016/j.epsl.2005.06.041

Zhao Jun, Zhang Haisheng, Wu Guanghai, et al. 2014. Biomineralization of organic matter in cobalt-rich crusts from the Marcus-Wake Seamounts of the western Pacific Ocean. Acta Oceanologica Sinica, 33(12): 67–74, doi: 10.1007/s13131-014-0552-0